Bicycle Drive System Dynamics: Theory and Experimental Validation

Benjamin J. Fregly
Department of Aerospace Engineering, Mechanics & Engineering Science, University of Florida, Gainesville, FL 32611

Felix E. Zajac
Rehabilitation R&D Center, Veterans' Affairs Palo Alto Health Care System, Palo Alto, CA 94304; and Departments of Mechanical Engineering (Biomechanical Engineering Division) & Functional Restoration, Stanford University, Stanford, CA 94305

Christine A. Dairaghi
Rehabilitation R&D Center, Veterans' Affairs Palo Alto Health Care System, Palo Alto, CA 94304

Bicycle pedaling has been studied from both a motor control and an equipment setup and design perspective. In both cases, although the dynamics of the bicycle drive system may have an influence on the results, a thorough understanding of the dynamics has not been developed. This study pursued three objectives related to developing such an understanding. The first was to identify the limitations of the inertial/frictional drive system model commonly used in the literature. The second was to investigate the advantages of an inertial/frictional/compliant model. The final objective was to use these models to develop a methodology for configuring a laboratory ergometer to emulate the drive system dynamics of road riding. Experimental data collected from the resulting road-riding emulator and from a standard ergometer confirmed that the inertial/frictional model is adequate for most studies of road-riding mechanics or pedaling coordination. However, the compliant model was needed to reproduce the phase shift in crank angle variations observed experimentally when emulating the high inertia of road riding. This finding may be significant for equipment setup and design studies where crank kinematic variations are important or for motor control studies where fine control issues are of interest.
[S0148-0731(00)02004-5]

Introduction

Researchers have studied bicycle pedaling to address equipment setup and design problems and motor control issues. From an equipment setup and design perspective, the ultimate goal is usually to improve human performance during outdoor riding. However, due to the difficulty of collecting data from a bicycle and rider on the road, most experimental pedaling studies have been performed in the laboratory using a mechanically braked ergometer [1–3], an electronically braked ergometer [4–6], a bicycle on roller cylinders [7–9], a Velodyne trainer [10–12] or a bicycle on a treadmill [13–16]. Numerous computer simulation studies of road riding have also been performed, for example, to determine optimal bicycle configuration and rider position [17,18], to design noncircular chainrings for improved pedaling efficiency [19–21], or to design off-road bicycle suspension systems [22]. An explicit dynamic model of a bicycle drive system is therefore desirable to assess how well various experimental situations mimic the dynamic loading of outdoor riding and to determine whether drive system models used in simulation studies of road riding are appropriate to the goal of the study.

From a motor control perspective, pedaling provides the investigator with the unique opportunity to manipulate the external load and study how the body responds. This approach requires that the mechanical characteristics of the external load be well understood so that changes in control strategy can be correlated with changes in the load. Historically, most experimental studies of pedaling coordination have manipulated the cadence [23–25], the frictional resistance [23,24,26], the cadence and frictional resistance simultaneously [5,6,8], or the bicycle gear ratio [8,11,27]. A few investigators have also manipulated the inertial resistance [28–30], but in general, the amount of inertia used in the experimental apparatus is rarely mentioned. Thus, the implicit assumption is often made that inertia, and therefore drive system dynamics, does not have an influence on pedaling coordination. A more through understanding of bicycle drive system dynamics is needed to assess the reasonableness of this assumption.

This study focuses on three objectives related to developing a better understanding of bicycle drive system dynamics. The first objective is to examine the limitations of the noncompliant drive system model commonly used (or implicitly assumed) in the pedaling literature. The second is to investigate the potential advantages of a more complex compliant model. The final objective is to develop a methodology, based on these models, for configuring a laboratory pedaling ergometer to emulate the drive system dynamics of outdoor riding. Experimental data collected from the resulting road-riding emulator and from a standard Monark ergometer served to test the models and to highlight when consideration of drive system dynamic effects may be important.

Methods

Noncompliant Model. A one degree-of-freedom inertial/frictional model (henceforth called the "noncompliant model") is the most common dynamic drive system model found in the literature [20,31–33]. The equation of motion for this model is

$$I_{\text{Eff}}\ddot{\theta}_1 = T_c - T_{\text{Eff}} \tag{1}$$

where

- I_{Eff} = effective rotational inertia about the crank axis due to rigid bodies rotating about the crank axis (i.e., the chainrings, pedals, and crank arms) and about the flywheel or rear wheel axis (e.g., the freewheel)
- θ_1 = angle of the crank measured with respect to top dead center
- T_c = crank torque due to the pedal forces produced by both legs
- T_{Eff} = effective resistance torque about the crank axis

There are two key assumptions inherent in this model. The first is that the bicycle drive system is infinitely stiff. Consequently, if the rear wheel were locked in place, no rotation of the crank arm would occur if a driving force were applied to the pedals. The second assumption is that the freewheel in the model cannot decouple from the flywheel or rear bicycle wheel, much like with a

Contributed by the Bioengineering Division for publication in the JOURNAL OF BIOMECHANICAL ENGINEERING. Manuscript received by the Bioengineering Division August 9, 1998; revised manuscript received March 22, 2000. Associate Technical Editor: M. L. Hull.

fixed-gear track bicycle. This assumption becomes invalid whenever the contact torque exerted by the freewheel on the flywheel or rear bicycle wheel goes to zero, which occurs if T_c becomes less than about 0.5 N·m [34].

Compliant Model. A slightly more complex two degree-of-freedom inertial/frictional/compliant model (henceforth called the "compliant model") can be obtained by eliminating the assumption that the bicycle drive system is infinitely stiff. In this situation, the equations of motion are

$$\begin{bmatrix} I_{\text{Crk}} & 0 \\ 0 & I_{\text{Ref}} \end{bmatrix}\begin{bmatrix} \ddot{\theta}_1 \\ \ddot{\theta}_2 \end{bmatrix}=\begin{bmatrix} T_c \\ 0 \end{bmatrix}-\begin{bmatrix} C_{\text{Eff}} & -C_{\text{Eff}} \\ -C_{\text{Eff}} & C_{\text{Eff}} \end{bmatrix}\begin{bmatrix} \dot{\theta}_1 \\ \dot{\theta}_2 \end{bmatrix} -\begin{bmatrix} K_{\text{Eff}} & -K_{\text{Eff}} \\ -K_{\text{Eff}} & K_{\text{Eff}} \end{bmatrix}\begin{bmatrix} \theta_1 \\ \theta_2 \end{bmatrix}-\begin{bmatrix} 0 \\ T_{\text{Eff}} \end{bmatrix} \quad (2)$$

where

I_{Crk} = rotational inertia about the crank axis due to rigid bodies rotating about this axis (i.e., the chainrings, pedals, and crank arms)
I_{Ref} = rotational inertia about the crank axis, as reflected through the gearing, due to rigid bodies rotating about the flywheel or rear wheel axis (e.g., the freewheel)
θ_2 = angle of the reflected inertial load measured with respect to top dead center
C_{Eff} = effective rotational damping about the crank axis
K_{Eff} = effective rotational stiffness about the crank axis

and θ_1, T_c, and T_{Eff} are as defined in Eq. (1). In this model, I_{Eff} is split into two components, I_{Crk} and I_{Ref}, separated by a torsional spring with stiffness K_{Eff}. This spring accounts for all compliances in the drive system (see Discussion), while the spring deflection $\theta_1-\theta_2$ is consistent with how K_{Eff} was measured experimentally (see below). When K_{Eff} goes to infinity, I_{Crk} and I_{Ref} respond as a single rigid body, and Eq. (2) reduces to Eq. (1) with $I_{\text{Eff}}=I_{\text{Crk}}+I_{\text{Ref}}$.

Dynamic Equivalence. These models were used to develop a methodology for configuring a laboratory pedaling ergometer to emulate the bicycle drive system dynamics of outdoor riding. Starting with the simpler noncompliant model, the relationship between the model parameters I_{Eff} and T_{Eff} and the physical properties (e.g., masses, inertias, radii, and gear ratio) of a standard ergometer or road bicycle can be determined from dynamics. A schematic of a standard ergometer is shown in Fig. 1(*a*), and the corresponding equation of motion can be shown to be

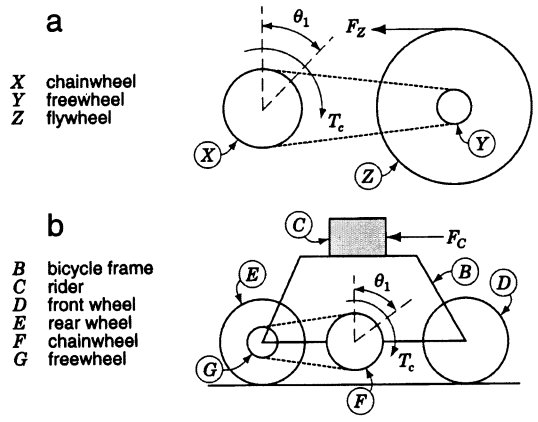

Fig. 1 Schematics of one degree-of-freedom bicycle drive systems: (*a*) Monark stationary bicycle ergometer; (*b*) twelve-speed road bicycle

$$\underbrace{\{I_X+(R_X/R_Y)^2(I_Y+I_Z)\}}_{(I_{\text{Eff}})_{\text{Ergometer}}}\ddot{\theta}_1=T_c-\underbrace{\{(R_X/R_Y)R_ZF_Z\}}_{(T_{\text{Eff}})_{\text{Ergometer}}} \quad (3)$$

where

I_X = combined rotational inertia of the chainring, pedals, and crank arms about the crank axis
I_Y, I_Z = rotational inertia of the ergometer freewheel and flywheel, respectively, about their axes of rotation
R_X/R_Y = gear ratio, which is 52/14 (i.e., 3.7:1) for a standard Monark ergometer
R_Z = radius of the ergometer flywheel
F_Z = frictional resistance force applied to the flywheel by the band brake

Similarly, Fig. 1(*b*) presents a schematic of a road bicycle, with a corresponding equation of motion

$$\underbrace{\{I_F+(R_F/R_G)^2[R_D^2(m_B+m_C+2m_D+m_F+m_G)+(2I_D+I_G)]\}}_{(I_{\text{Eff}})_{\text{Road}}}\ddot{\theta}_1 =T_c-\underbrace{\{(R_F/R_G)R_DF_C\}}_{(T_{\text{Eff}})_{\text{Road}}} \quad (4)$$

where

m_B, m_C, m_D, m_G = mass of the bicycle frame, the rider, each bicycle wheel, and the freewheel, respectively
m_F = mass of the chainrings, crank arms, and pedals, collectively
I_D = rotational inertia of each bicycle wheel about its axis of rotation
I_F = combined rotational inertia of the chainrings, pedals, and crank arms about the crank axis
I_G = rotational inertia of the freewheel about its axis of rotation
R_D = radius of each bicycle wheel
R_F/R_G = gear ratio, which ranges from 42/28 (i.e., 1.5:1) to 52/13 (i.e., 4:1) for many 12-speed road bicycles
F_C = total opposing force experienced by the rider due to wind and rolling resistance and chain and bearing friction

The drive system dynamics for a bicycle on roller cylinders can also be expressed in the form of Eq. (1) [35]. Equations (3) and (4) indicate that T_{Eff} is a linear function and I_{Eff} a quadratic function of the selected gear ratio. For an infinitely stiff drive system, Eqs. (1), (3), and (4) suggest that a stationary ergometer could be configured to match the dynamic response of a road bicycle by setting $(I_{\text{Eff}})_{\text{Ergometer}}=(I_{\text{Eff}})_{\text{Road}}$ and $(T_{\text{Eff}})_{\text{Ergometer}}=(T_{\text{Eff}})_{\text{Road}}$. Drive system compliance introduces the additional requirements that $(K_{\text{Eff}})_{\text{Ergometer}}=(K_{\text{Eff}})_{\text{Road}}$ and $(C_{\text{Eff}})_{\text{Ergometer}}=(C_{\text{Eff}})_{\text{Road}}$.

This theory can be simplified by realizing that I_{Eff} and T_{Eff} in Eq. (4) ultimately depend on only two parameters: road-riding cadence and gear ratio. The I_{Eff} expression only depends on bicycle and rider physical properties (i.e., masses, inertias, radii, and gear ratio). The T_{Eff} expression depends on radii and F_C, which can be estimated as a function of gear ratio and cadence from information reported by Whitt and Wilson [36] (see below). Consequently, substituting an expression for F_C and the physical properties of a nominal bicycle-rider situation (see [34] for details) into Eq. (4) produces the following simplified expressions for road-riding I_{Eff} and T_{Eff}:

$$I_{\text{Eff}}(\text{kg}\cdot\text{m}^2)\approx 3.456\times 10^{-2}+10.442g_r^2$$
$$T_{\text{Eff}}(\text{N}\cdot\text{m})\approx 2.125g_r+1.379\times 10^{-4}g_r^3\ \text{rpm}^2 \quad (5)$$

where

g_r = gear ratio, expressed as teeth in chainring divided by teeth in freewheel

rpm = cadence in revolutions per minute

Because F_C is a quadratic function of g_r, this simplified expression for T_{Eff} is a cubic rather than linear (i.e., as suggested by Eq. (4)) function of g_r. Since work rate is simply T_{Eff} multiplied by cadence, and since road-riding speed only depends on tire radius, cadence, and gear ratio, we also have:

$$\text{Work rate (W)} \approx 2.225\times10^{-1}\, g_r\,\text{rpm} + 1.444\times10^{-5}\, g_r^3\,\text{rpm}^3$$

$$\text{Speed(m/s)} \approx 3.591\times10^{-2} g_r\,\text{rpm} \qquad (6)$$

For constant speed pedaling through still air on a level grade, the work rate relationship in Eq. (6) (if re-expressed as a function of road-riding speed) is of the same form as that developed by Martin et al. [37]. However, their equation is more precise since it accounts for a wider variety of frictional effects (e.g., road grade) and was validated using experimental data collected during actual road riding.

Equations (5) and (6) were used in the present study to estimate ergometer-equivalent I_{Eff} and T_{Eff} values for a typical tourist cycling situation. Their dependence on only g_r and rpm makes them suitable for other studies seeking to emulate various road-riding scenarios. The I_{Eff} expression assumes a 50th percentile U.S. male rider (77.8 kg) pedaling a Trek 560 road bicycle (12.3 kg). For the standard gearing available on many 12-speed bicycles, I_{Eff} ranges from about 24 kg·m^2 (a 42/28 gear ratio) to around 167 kg·m^2 (a 52/13 gear ratio). The T_{Eff} expression is derived from information for wind drag, rolling resistance, and chain and bearing friction [36] and assumes pedaling through still air. The wind resistance calculation assumes a tourist cyclist with a drag coefficient of 1.0 and frontal area of 0.5 m^2. The rolling resistance calculation utilizes a tire pressure of 0.5 MPa (75 psi). The bicycle transmission was assumed to be 95 percent efficient.

Experiments. Four experimental cases, which were combinations of two I_{Eff} and two T_{Eff} values (see Table 1), were used to test the models. The larger I_{Eff} value of 101.6 kg·m^2 was representative of a 50th percentile U.S. male rider pedaling a 12-speed road bicycle in a 52/17 gear ratio. This high inertia was achieved by connecting a single ergometer flywheel to the crank through three-stage gearing with an overall gear ratio of 16.4:1 (Fig. 2(*a*)). The resulting inertia was slightly greater than the desired 97.7 kg·m^2 (substitute 52/17 into Eq. (5)) due to limited gear ratio resolution. The smaller I_{Eff} value of 5.2 kg·m^2 was representative of a standard Monark ergometer. This inertia, which was included for comparison purposes, was achieved by connecting a separate flywheel to the crank through single-stage gearing using the standard Monark gear ratio of 3.7:1 (Fig. 2(*b*)). The two T_{Eff} values corresponded to two recreational road-riding cadences in the specified gear ratio (see Eq. (5)). The lower cadence of 60 rpm corresponds to a T_{Eff} value of 20.7 N·m, a road-riding work rate of 130 W, and a road-riding speed of 6.6 m/s; the higher cadence of 75 rpm to a T_{Eff} value of 28.7 N·m, a work rate of 225 W, and a speed of 8.2 m/s (see Eq. (6)). For all four cases, C_{Eff} was assumed to be small, and K_{Eff} was adjusted to be about 3000 N·m/rad, close to that of a road bicycle in a 52/17 gear ratio (see Discussion).

Table 1 Summary of the four experimental pedaling conditions

Emulated Pedaling Situation	I_{Eff} (kg·m^2)	T_{Eff} (N·m)	K_{Eff} (N·m/rad)	Cadence (rpm)	Work rate (Watts)
Road bicycle in 52/17 gear ratio	101.6	20.7	3000	60	130
Monark ergometer	5.2	20.7	3000	60	130
Road bicycle in 52/17 gear ratio	101.6	28.7	3000	75	225
Monark ergometer	5.2	28.7	3000	75	225

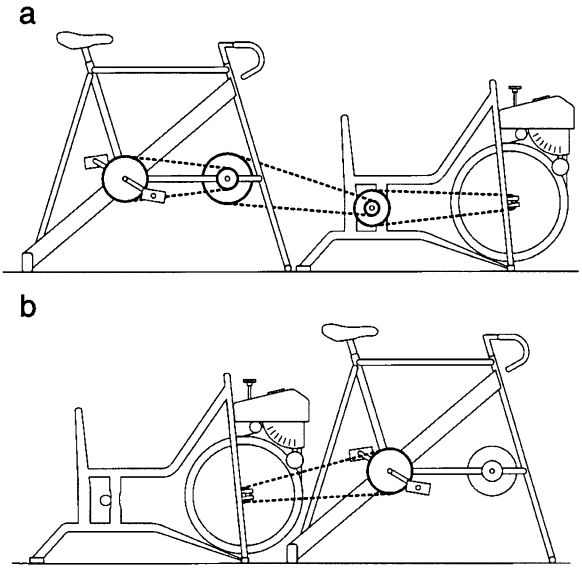

Fig. 2 Pedaling apparatus configurations to achieve two effective drive system inertias: (*a*) high-inertia configuration to emulate a 12-speed road bicycle in a 52/17 gear ratio with a 50th percentile U.S. male rider. The translational inertia of the rider is accounted for in the rotational inertia of the experimental drive system. (*b*) Low inertia configuration to emulate a standard Monark 868 ergometer.

Details of the experimental data collection have been reported previously [28,34]. Briefly, ten recreational male cyclists gave informed consent and performed all four cases (one trial per case) during a single session. To study the frequency response of both drive systems, we had one additional subject pedal over a range of cadences from 20 and 100 rpm. The protocol for the experiments was approved according to the relevant laws and regulations of Stanford University. Subject position emulated road riding by using a seat tube angle of 73 deg, a crank arm length of 0.170 m, a standard road bicycle seat and handlebars, and cleated cycling shoes with toe clips. Cadence feedback was provided by a cycle computer mounted on the handlebars. Compressive and shear forces applied by the subject to the surface of the right and left pedals were measured using two pedal dynamometers [38], while crank arm orientation with respect to the seat tube and pedal orientation with respect to each crank arm were measured using rotary optical encoders. A sampling frequency of 1000 Hz was used for all data.

To provide data for model evaluation, we calculated the crank torque and the crank angle residual (defined below) from measured quantities. The crank torque from both legs was computed from the known crank arm length and the right and left pedal forces perpendicular to the crank arm. The crank angle residual, defined as the variation in crank angle from a linear function of time, was calculated from the relationship $\theta_r = \theta_c - (360/t_f)t$, where θ_c is the crank angle, t is the time from the start of the cycle, and t_f is the final time of the cycle. The crank angle was defined to be zero at top dead center, which corresponds to the start of the cycle. One representative data set was created for each of the four experimental cases by averaging from each subject the ten consecutive cycles whose average cadence was closest to the specified cadence.

Fourier analysis was used to eliminate high-frequency noise from the averaged periodic data [39]. Crank torque curves were smoothed using ten harmonics, capturing 99 percent of the signal power in all cases. Crank angle residual curves were smoothed using four harmonics, which captured between 72 and 88 percent of the signal power in all cases. While more harmonics captured

more of the signal power, unrealistic estimates of crank angular velocity and acceleration then resulted. Furthermore, the magnitude of the residual curves was quite small, with the root-mean-square (rms) error between a smoothed and unsmoothed curve being less than 0.03 deg.

Analyses. Two different approaches were used to evaluate the ability of the models to reproduce the experimental data. The first approach was to perform a dynamic simulation for each of the four experimental cases. To fine-tune the simulations, we used a parameter optimization approach [40] to adjust the crank torque and initial condition inputs as little as possible to reproduce the observed crank angle residual output. The minor crank torque adjustment accounts for the ± 4 N·m of variability present in the averaged data. The initial condition change was primarily in the compliant model's torsional spring deflection, which was not measured experimentally. The second approach was to compute bode frequency response plots (gain and phase) for the experiments and the models, where the crank angle residual was the output and the crank torque the input. Since two cycles of crank torque occur for each crank revolution, a conversion factor of $15/\pi$ was required to convert frequency from rad/s to rpm. For the experiments, the crank angle residual and crank torque were approximated from the dominant second harmonic, and gain was computed by dividing the output magnitude by the input magnitude and taking $20 \log_{10}$ of the result. For the models, gain and phase were computed from the appropriate transfer function (see appendix for details) using the "bode" command of MATLAB®. To improve the match between the compliant model and the experiments, we made small adjustments to I_{Eff}, K_{Eff}, and C_{Eff} using a MATLAB® nonlinear least squares routine. A discussion of the transition frequency ω_z appearing in the frequency response plots can be found in the appendix.

Results

The noncompliant drive system model was limited in its ability to reproduce the experimental results. For emulated road riding, the simulated crank angle residual from this model showed large errors relative to the experiments (0.22 deg rms error at the low cadence and 0.41 deg rms error at the high one), in part due to an inversion in the phasing (Figs. 3(*a*,*b*), compare solid lines and dotted lines). While the model was able to reproduce the phasing of the experiments for emulated ergometer pedaling, the gain agreement was still better at the lower cadence (0.12 deg versus 0.22 deg rms error; Figs. 4(*a*,*b*), compare solid lines and dotted lines). These results can be explained by the frequency response plots, which showed that the model was unable to reproduce the phase shift observed experimentally in both drive systems. Consequently, the model tracked the experimental gain and phase results only at cadences below the transition frequency ω_z (Figs. 5(*a*,*b*), compare triangles and dotted lines). These discrepancies are probably unrelated to the hard-coupled freewheel assumption, since the crank torque in all experiments remained positive and greater than 5 N·m.

In contrast, the compliant model exhibited none of these limitations, suggesting that drive system compliance was the primary missing element. This model was able to reproduce the amplitude (to within 0.05 deg rms error) and phasing of the experimental crank angle residual for both emulated road riding (Figs. 3(*a*,*b*), compare solid lines and dashed lines) and emulated ergometer pedaling (Figs. 4(*a*,*b*), compare solid lines and dashed lines). In addition, it was able to reproduce the gain and phase transitions

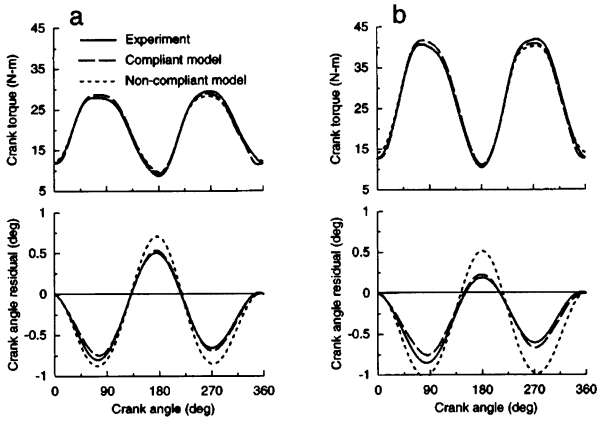

Fig. 4 Comparison of experimental and simulated trajectories for standard ergometer pedaling: (*a*) low cadence/work rate combination of 60 rpm/120 W; (*b*) high cadence/work rate combination of 75 rpm/225 W. Crank torque input is on the top, and variation in crank angle (i.e., "residual") output is on the bottom. Both models tracked the experimental crank torque and crank angle residual trajectories reasonably well.

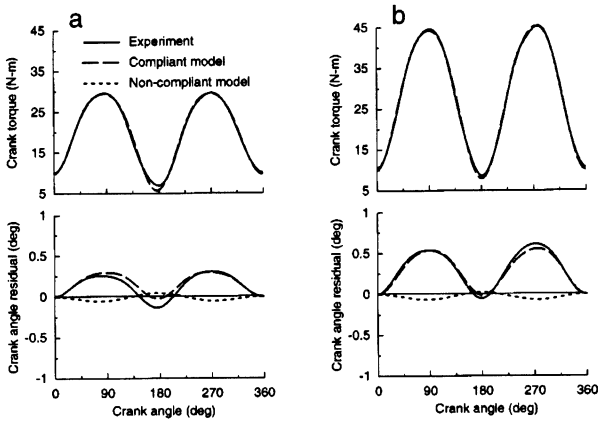

Fig. 3 Comparison of experimental and simulated trajectories for emulated road riding: (*a*) low cadence/work rate combination of 60 rpm/120 W: (*b*) high cadence/work rate combination of 75 rpm/225 W; Crank torque input is on the top, and variation in crank angle (i.e., "residual") output is on the bottom. Only the compliant model tracked the experimental crank torque and crank angle residual trajectories simultaneously.

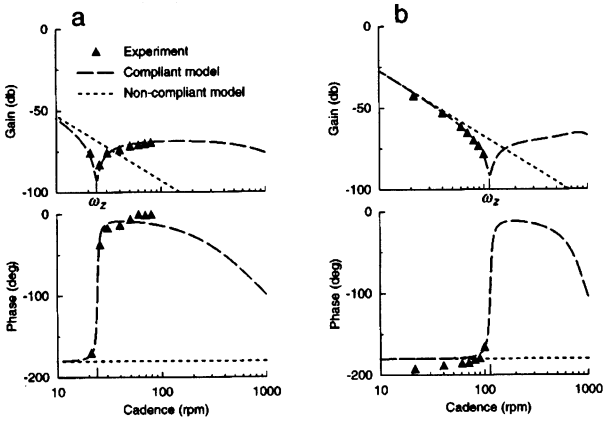

Fig. 5 Comparison of experimental and simulated bode frequency response: (*a*) emulated road riding; (*b*) standard ergometer pedaling. Gain is on the top, and phase is on the bottom. The compliant model tracked the experimental frequency response extremely well, while the noncompliant model tracked it only below the frequency ω_z defined by the compliant model's transfer function zero.

observed in the frequency response experiments for both drive systems (Figs. 5(*a*,*b*), compare triangles and dashed lines). Thus, the compliant model could reproduce the experimental data at all cadences above and below the transition frequency. Note that in all optimizations with both models, the rms change in crank torque was never greater than 1 N·m.

Finally, due to the significantly larger drive system inertia achieved for emulated road riding, the experimental results for this situation exhibited obvious differences from those of emulated ergometer pedaling. For the same cadence and effective resistance torque, the phasing of the crank angle residual was opposite in the two drive systems, contributing to the large overall differences in the residual curves (0.63 deg rms difference at the low cadence and 0.80 deg at the high one; compare Fig. 3(*a*) with Fig. 4(*a*) and Fig. 3(*b*) with Fig. 4(*b*), solid lines). Although the shapes of the gain and phase frequency response curves were similar for the two situations, the transition frequency ω_z was much lower for emulated road riding than for emulated ergometer pedaling (25 rpm versus 105 rpm; compare Figs. 5(*a*) and 5(*b*), triangles).

Discussion

This study pursued three objectives related to the understanding bicycle drive system dynamics. The motivation for pursuing these objectives was to determine under what conditions the experimental and computer modeling approaches found in the literature are appropriate for studying road riding mechanics or motor control issues.

An important finding of this study is that though somewhat limited in its capabilities, the commonly used noncompliant drive system model appears to be fully adequate for many pedaling investigations. Regardless of how much drive system inertia was used in the experimental apparatus, the crank angle residual was small in all cases (at most about ±1 deg), suggesting that the additional complexity required to model drive system compliance may not be worth the effort. However, the hard-coupled freewheel assumption limits use of the model to situations where coasting or extremely "choppy" pedaling does not occur. Thus, the noncompliant drive system model appears to be appropriate for most studies of road-riding mechanics or pedaling coordination.

Despite this statement, there may still be situations where the extra fidelity provided by the compliant drive system model is important. For equipment setup and design problems, this extra fidelity may be necessary in situations where variations in the crank kinematics are important. One such situation might be the design of noncircular chainrings, where the goal is to create a variable crank angular velocity profile to improve pedaling efficiency [19–21]. In this situation, the crank angular velocity variations would be much larger than those encountered with the circular chainring used in our study. A noncircular chainring designed under the assumption of an infinitely stiff drive system would not take into account the phase shift in crank kinematics. As a result, the chainring shape as well as the orientation of the major and minor axes could be affected. Another area where crank kinematic variations may have an influence is the design of off-road bicycle suspension systems. The variable chainstay length in such suspensions may reduce the effective stiffness of the drive system, thereby lowering the transition frequency and causing a phase lag in the suspension deflections even at extremely low cadences. Such a lag was observed by Wang and Hull [22].

A more accurate drive system model may also be useful for studying certain motor control issues. For example, one could study fine coordination of pedaling by varying I_{Eff} and K_{Eff}. Fregly et al. [28] found that only the net ankle muscle joint torque exhibited statistically significant changes when the ergometer drive system inertia was increased 20-fold. Since these changes could not be explained by differences in work rate or cadence, Fregly and co-authors hypothesized that they were due to fine motor control adjustments of the ankle muscles in response to the altered drive system dynamics. A detailed analysis of changes in muscle EMG activity would be required to investigate this possibility further.

A valuable feature of the compliant model is that it can be used to predict when the noncompliant model is adequate, even in situations where crank kinematic variations or fine motor control issues are of interest. This is possible because the transfer function of the compliant model can be used to derive the following mathematical expression for the transition frequency w_z (see appendix for derivation):

$$w_z\,(\text{in rpm}) \approx \sqrt{\frac{K_{\text{Eff}}}{I_{\text{Eff}}}} \times \frac{15}{\pi} \tag{7}$$

Our results suggest that the noncompliant model will provide a good representation of the drive system dynamics as long as the selected cadence is well below this frequency. How far below depends on the amount of damping in the drive system, which can be estimated by tuning C_{Eff} in the compliant model's transfer function (see appendix) to match the frequency response of the experimental drive system.

The dynamic equivalence methodology derived from these drive system models contains several important assumptions, which should be considered. One important assumption was that the compliant model provided an adequate representation of a road bicycle drive system. We cannot claim with certainty that our road-riding emulator reproduced the drive system dynamics of a road bicycle, since we did not collect comparable data during actual road riding. Without such data, we can only state with certainty that the methodology is self-consistent, since the compliant model was able to reproduce all of our experimental results. The strength of this statement should not be minimized, however, since we could not make it based on the noncompliant model. This self-consistency between the compliant model and the experimental results therefore suggests that the road-riding emulator provided a reasonable representation of the actual situation.

Two assumptions related to I_{Eff} for road riding were inherent in the methodology. The first was that the rotational inertia of the rider's limbs does not contribute to the effective drive system inertia. Since the majority of road-riding I_{Eff} comes from the translational inertia of the bicycle and rider, this simplifying assumption is not expected to have a significant influence on the calculated I_{Eff} value. The second assumption was that the rotational inertia I_Y of the flywheel was known precisely. Because I_Y is multiplied by the gear ratio squared in Eq. (3), use of a large ergometer gear ratio to emulate road riding makes I_{Eff} sensitive to errors in I_Y. Our frequency response results suggest that our initial estimate of I_Y was probably about 0.02 kg·m^2 (or approximately 5 percent) too low. Consequently, I_{Eff} for our road-riding emulator may have been 5 kg·m^2 (or 5 percent) larger than calculated.

An important assumption related to T_{Eff} was that the specified values could be set accurately on the road-riding emulator. When a large ergometer gear ratio is used, setting T_{Eff} accurately becomes difficult for two reasons. First, T_{Eff} becomes much more sensitive to errors in the flywheel friction setting (review Eq. (3)), since a smaller amount of belt friction is required to achieve the same value of T_{Eff}. Second, flywheel wind friction effects become important, since the flywheel angular speed is extremely high even for moderate cadences. To address these issues, we geared a rotary potentiometer to the band brake pendulum of the flywheel, thereby improving the resolution with which the band brake friction could be measured. Output from the potentiometer was calibrated with T_{Eff} using bilateral pedal force measurements. In this way, the resulting calibration curves accounted for not only flywheel belt friction, but also bearing friction, chain friction, flywheel wind friction, and any other frictional effects experienced

Table 2 Estimated drive system inertia values for common laboratory pedaling situations relative to road riding. I_{Eff} min assume a bicycle gear ratio of 42/28, while I_{Eff} max assumes a gear ratio of 52/13. The gear ratio of a standard Monark ergometer is fixed at 52/14.

Pedaling Situation	I_{Eff} min (kg·m²)	I_{Eff} max (kg·m²)
Monark ergometer	5.2	5.2
Bicycle on rollers	2.0	13.9
Velodyne trainer	16.0	113.7
Road bicycle	23.5	167.1

by the rider at the crank. Statistical analysis of the average experimental crank torque verified the accuracy of the calibration curves [28].

A final assumption was that the torsional spring stiffness K_{Eff} could be set to match that of a road bicycle in the specified gear ratio. To determine K_{Eff} for a road bicycle, we mounted a Trek 560 racing bicycle on a turbo trainer stand, locked the rear wheel, and measured the amount of crank deflection due to a range of applied crank torques. Crank deflection was measured using a video-based motion analysis system, while crank torque was determined from a single pedal force transducer. For a 52/18 gear ratio, we found K_{Eff} to be approximately 3000 N·m/rad ($r^2 > 0.979$ for the two trials). To attempt to model this compliance, we investigated whether chain compliance accounts for the majority of $1/K_{Eff}$. Based on a theoretical relationship for how chain stretch translates into rotation about the crank axis (see [34] for details), we calculated that K_{Eff} due to chain compliance alone was approximately 8650 N·m/rad, or about a third of the effective compliance. The remaining compliance comes from a variety of sources that are difficult to model, such as bending of the sprockets, bending of the axles, and flexing of the frame. Nonetheless, this relationship indicated that K_{Eff} could be increased by using a larger front sprocket, a shorter tensioned length of chain, or a chain with greater stiffness per link. In the present study, this information was used to select bicycle chains with different stiffness properties so as to achieve the desired K_{Eff} value on the road-riding emulator. Stiffness per link for twelve different chain models as measured with an MTS machine is reported in Fregly [34].

An important benefit of the dynamic equivalence methodology is that it provides a theoretical basis for assessing how various laboratory pedaling situations compare to road riding. Of the three parameters in the compliant model, the effective drive system inertia I_{Eff} is the most likely to vary widely. Table 2 presents our estimates of I_{Eff} for several typical laboratory pedaling situations relative to road riding. Only one common apparatus, the Velodyne trainer (Collinear Research Corporation, Irvine, CA), comes close to matching this aspect of road riding, producing 68 percent of the inertia of road riding in the same gear ratio [41]. Similar to our road-riding emulator, the Velodyne achieves its high inertia mechanically by gearing up a flywheel. While electronically braked ergometers are more sophisticated than their mechanically braked counterparts, their control algorithms only affect T_{Eff} by applying a braking force to emulate wind resistance, rolling resistance, chain and bearing friction, and gravitational resistance. Emulating I_{Eff} electronically rather than mechanically would require acceleration feedback and a servo motor rather than just a braking device.

As an example of this methodology, consider how dynamic equivalence would be used to evaluate a typical laboratory pedaling scenario. We will assume that this hypothetical experiment is performed on a Monark ergometer ($I_{Eff}=5.2\,kg\cdot m^2$) using a cadence of 90 rpm and a work rate of 200 W ($T_{Eff}=21.2\,N\cdot m$), conditions similar to many pedaling experiments found in the literature. From the I_{Eff} expression in Eq. (5), a road bicycle gear ratio of 26/37 would be required to emulate the low inertia of $5.2\,kg\cdot m^2$. With the gear ratio specified to meet the inertia requirement, the T_{Eff} expression in Eq. (6) yields a corresponding resistance torque of only 1.9 N·m. To increase T_{Eff} to the required 21.2 N·m, the rider would also have to pedal against a 14.0 m/s head wind. Thus, many ergometer pedaling experiments correspond to road riding in an extremely low gear ratio against an extremely high head wind.

In conclusion, we have demonstrated the limitations of the noncompliant drive system model commonly used in the literature, proposed a compliant model to overcome these limitations, and developed a methodology based on these models for configuring a laboratory pedaling ergometer to emulate the drive system dynamics of any specified road riding situation. While our findings may not be significant for many pedaling situations, researchers should be aware of when inertial and compliance effects may influence experimental or computer modeling results. This is most likely to be the case in equipment setup and design studies where crank kinematic variations are important and in motor control studies where fine control issues are of interest.

Acknowledgments

This work is derived from a Ph.D. dissertation [34], which was supported by NIH grant NS17662 and the Rehabilitation R&D Service of the Department of Veterans Affairs. We thank Greg Woodward for his insights into dynamic equivalence, Erin Catto for his help with frequency response analysis, Jim Anderson and Doug Schwandt for their assistance with apparatus design and construction, and Steve Kautz for his very helpful comments on a previous version of the manuscript.

Appendix

Both dynamic drive system models can be evaluated over a wide range of cadences by plotting their bode frequency response curves from their respective transfer functions, where the output is the periodic crank angle θ_1 and the input is the periodic crank torque T_c.

For the noncompliant model, the transfer function between θ_1 and T_c can be found analytically by taking the Laplace transform of Eq. (1) and performing some algebraic manipulations:

$$G_1(s)=\frac{\theta_1(s)}{T_c(s)}=\frac{1}{I_{Eff}s^2} \tag{A1}$$

This transfer function possesses no zeros and two poles at the s-plane origin, indicating that the only natural frequency is zero. Consequently, only rigid body motion is possible, and the output and input will always be out of phase for harmonic excitation (see Fig. 5, dotted lines).

For the compliant model, the transfer function between θ_1 and T_c can be found from Eq. (2) by following a similar process:

$$G_2(s)=\frac{\theta_1(s)}{T_c(s)}=\frac{I_{Ref}s^2+C_{Eff}s+K_{Eff}}{s^2[I_{Crk}I_{Ref}s^2+(I_{Crk}+I_{Ref})C_{Eff}s+(I_{Crk}+I_{Ref})K_{Eff}]} \tag{A2}$$

The characteristic frequencies can then be determined by setting C_{Eff} to zero. From the poles, this yields natural frequencies at zero (i.e., the system is semidefinite) and $\omega_p=\sqrt{(I_{Crk}+I_{Ref})K_{Eff}/(I_{Crk}I_{Ref})}$, while from the zeros, a frequency

at $\omega_z = \sqrt{K_{Eff}/I_{Ref}}$. Since $I_{Ref} \gg I_{Crk} \approx 0$, the one nonzero natural frequency ω_p will always be much higher than ω_z, so that the main effects can be seen by setting I_{Crk} to zero:

$$G_2(s) = \frac{\theta_1(s)}{T_c(s)} \approx \frac{1}{K_{Eff}} \frac{s^2 + \omega_z^2}{s^2} \tag{A3}$$

For harmonic excitation, Eq. (A3) indicates that the output and input will be out of phase below ω_z and in phase above it, while the gain will be minimum at ω_z (see Fig. 5, dashed lines).

References

[1] Coast, R. J., and Welch, H. G., 1985, "Linear Increase in Optimal Pedal Rate With Increased Power Output in Cycle Ergometry," Eur. J. Appl. Physiol., **53**, pp. 339–342.

[2] Henderson, S. C., Ellis, R. W., Klimovitch, G., and Brooks, G. A., 1977, "The Effects of Circular and Elliptical Chainwheels on Steady-Rate Cycle Ergometer Work Efficiency," Med. Sci. Sports, **9**, pp. 202–207.

[3] Kautz, S. A., Feltner, M. E., Coyle, E. F., and Baylor, A. M., 1991, "The Pedaling Technique of Elite Endurance Cyclists: Changes With Increasing Workload at Constant Cadence," Int. J. Sport Biomech. **7**, pp. 229–253.

[4] Billat, V. L., Richard, R., Binsse, V. M., Koralsztein, J. P., and Haouzi, P., 1998, "The VO_2 Slow Component for Severe Exercise Depends on Type of Exercise and Is Not Correlated With Time to Fatigue," J. Appl. Physiol., **85**, pp. 2118–2124.

[5] Patterson, R. P., and Moreno, M. I., 1990, "Bicycle Pedalling Forces as a Function of Pedalling Rate and Power Output," Med. Sci. Sports Exerc., **22**, pp. 512–516.

[6] Takaishi, T., Yasuda, Y., and Moritani, T., 1994, "Neuromuscular Fatigue During Prolonged Pedalling Exercise at Different Pedalling Rates," Eur. J. Appl. Physiol., **69**, pp. 154–158.

[7] Bolourchi, F., and Hull, M. L., 1985, "Measurement of Rider Induced Loads During Simulated Bicycling," Int. J. Sport Biomech., **1**, pp. 308–329.

[8] Hull, M. L., and Jorge, M., 1985, "A Method for Biomechanical Analysis of Bicycle Pedalling," J. Biomech., **18**, pp. 631–644.

[9] Nordeen-Snyder, K. S., 1977, "The Effect of Bicycle Seat Height Variation Upon Oxygen Consumption and Lower Limb Kinematics," Med. Sci. Sports Exerc., **9**, pp. 113–117.

[10] Hull, M. L., Williams, M., Williams, K., and Kautz, S., 1992, "Physiological Response to Cycling With Both Circular and Noncircular Chainrings," Med. Sci. Sports Exerc., **24**, pp. 1114–1122.

[11] Marsh, A. P., and Martin, P. E., 1995, "The Relationship Between Cadence and Lower Extremity EMG in Cyclists and Noncyclists," Med. Sci. Sports Exerc., **27**, pp. 217–225.

[12] Ruby, P., Hull, M. L., and Hawkins, D., 1992, "Three-Dimensional Knee Joint Loading During Seated Cycling," J. Biomech., **25**, pp. 41–53.

[13] Hagberg, J. M., Mullin, J. P., Giese, M. D., and Spitznagel, E., 1981, "Effect of Pedaling Rate on Submaximal Exercise Responses of Competitive Cyclists," J. Appl. Physiol., **51**, pp. 447–451.

[14] Stone, C., and Hull, M. L., 1993, "Rider/Bicycle Interaction Loads During Standing Treadmill Cycling," J. Appl. Biomech., **9**, pp. 202–218.

[15] Swain, D. P., and Wilcox, J. P., 1992, "Effect of Cadence on the Economy of Uphill Cycling," Med. Sci. Sports Exerc., **24**, pp. 1123–1127.

[16] Tanaka, H., Bassett, Jr., D. R., Best, S. K., and Baker, Jr., K. R., 1996, "Seated Versus Standing Cycling in Competitive Road Cyclists: Uphill Climbing and Maximal Oxygen Uptake," Can. J. Appl. Physiol., **21**, pp. 149–154.

[17] Gonzalez, H., and Hull, M. L., 1989, "Multivariable Optimization of Cycling Biomechanics," J. Biomech., **22**, pp. 1151–1161.

[18] Yoshihuku, Y., and Herzog, W., 1990, "Optimal Design Parameters of the Bicycle-Rider System for Maximal Muscle Power Output," J. Biomech., **23**, pp. 1069–1079.

[19] Hull, M. L., Kautz, S. A., and Beard, A., 1991, "An Angular Velocity Profile in Cycling Derived From Mechanical Energy Analysis," J. Biomech., **24**, pp. 577–586.

[20] Kautz, S. A., and Hull, M. L., 1995, "Dynamic Optimization Analysis for Equipment Setup Problems in Endurance Cycling," J. Biomech., **28**, pp. 1391–1401.

[21] Miller, N. R., and Ross, D., 1980, "The Design of Variable-Ratio Chain Drives for Bicycles and Ergometers—Application to a Maximum Power Bicycle Drive," ASME J. Mech. Des., **102**, pp. 711–717.

[22] Wang, E. L., and Hull, M. L., 1996, "A Model for Determining Rider Induced Energy Losses in Bicycle Suspension Systems," Vehicle Syst. Dynam. **25**, pp. 223–246.

[23] Citterio, G., and Agostoni, E., 1984, "Selective Activation of Quadriceps Muscle Fibers According to Bicycling Rate," J. Appl. Physiol., **57**, pp. 371–379.

[24] Duchateau, J., Le Bozec, S., and Hainaut, K., 1986, "Contributions of Slow and Fast Muscles of Triceps surae to a Cyclic Movement," Eur. J. Appl. Physiol., **55**, pp. 476–481.

[25] Suzuki, S., Watanabe, S., and Homma, S., 1982, "EMG Activity and Kinematics of Human Cycling Movements at Different Constant Velocities," Brain Res., **240**, pp. 245–258.

[26] Gregor, R. J., Komi, P. V., Browning, R. C., and Järvinen, M., 1991, "A Comparison of the *Triceps surae* and Residual Muscle Moments at the Ankle During Cycling," J. Biomech., **24**, pp. 2287–2297.

[27] Jorge, M., and Hull, M. L., 1986, "Analysis of EMG Measurement During Bicycle Pedalling," J. Biomech., **19**, pp. 683–694.

[28] Fregly, B. J., Zajac, F. E., and Dairaghi, C. A., 1996, "Crank Inertial Load Has Little Effect on Steady-State Pedaling Coordination," J. Biomech., **29**, pp. 1559–1567.

[29] Löllgen, H., Ulmer, H.-V., Gross, R., Wilbert, G., and van Nieding, G., 1975, "Methodical Aspects of Perceived Exertaion Rating and Its Relation to Pedalling Rate and Rotating Mass," Eur. J. Appl. Physiol., **34**, pp. 205–215.

[30] Patterson, R. P., and Pearson, J. L., 1983, "The Influence of Flywheel Weight and Pedalling Frequency on the Biomechanics and Physiological Responses to Bicycle Exercise," Ergonomics, **26**, pp. 659–668.

[31] Fregly, B. J., and Zajac, F. E., 1996, "A State-Space Analysis of Mechanical Energy Generation, Absorption, and Transfer During Pedaling," J. Biomech., **29**, pp. 81–90.

[32] Neptune, R. R., and Hull, M. L., 1998, "Evaluation of Performance Criteria for Simulation of Submaximal Steady-State Cycling Using a Forward Dynamic Model," ASME J. Biomech. Eng., **120**, pp. 334–340.

[33] Raasch, C. C., Zajac, F. E., Ma, B., and Levine, W. S., 1997, "Muscle Coordination of Maximum-Speed Pedaling," J. Biomech., **30**, pp. 595–602.

[34] Fregly, B. J., 1993, "The Significance of Crank Load Dynamics to Steady-State Pedaling Biomechanics: an experimental and Computer Modeling Study," Ph.D. dissertation, Stanford University, Stanford, CA.

[35] Fregly, B. J., and Zajac, F. E., 1989, "A Dynamical, Two-Legged Biomechanical Model to Study the Neuromuscular Control of Pedaling," in: *Issues in the Modeling and Control of Biomechanical Systems*, Stein, J. L., Ashton-Miller, J. A., and Pandy, M. G., eds., ASME DSC-Vol. 17, pp. 29–33.

[36] Whitt, F. R., and Wilson, D. G., 1990, *Bicycling Science*, MIT Press, Cambridge, MA.

[37] Martin, J. C., Milliken, D. L., Cobb, J. E., McFadden, K. L., and Coggan, A. R., 1998, "Validation of a Mathematical Model for Road Cycling Power," J. Appl. Biomech., **14**, pp. 276–291.

[38] Newmiller, J., Hull, M. L., and Zajac, F. E., 1988, "A Mechanically Decoupled Two Force Component Bicycle Pedal Dynamometer," J. Biomech., **21**, pp. 375–386.

[39] Winter, D. A. 1979, *Biomechanics of Human Movement*, J Wiley, New York.

[40] Pandy, M. G., Anderson, F. C., and Hull, D. G., 1992, "A Parameter Optimization Approach for the Optimal Control of Large-Scale, Musculoskeletal Systems," ASME J. Biomech. Eng., **114**, pp. 450–460.

[41] Sargeant, B., 1999 Personal communication regarding inertial properties of the Velodyne trainer.